Cheng-Kai ChiuHuang[1]
Mechanical and Aerospace
Engineering Department,
North Carolina State University,
R3311 Engineering Building 3,
Campus Box 7910, 911 Oval Drive,
Raleigh, NC 27695
e-mail: cchiuhu@ncsu.edu

Chuanzhen Zhou
Analytical Instrumentation Facility,
North Carolina State University,
Raleigh, NC 27695

Hsiao-Ying Shadow Huang
Mechanical and Aerospace
Engineering Department,
North Carolina State University,
R3311 Engineering Building 3,
Campus Box 7910, 911 Oval Drive,
Raleigh, NC 27695

In Situ Imaging of Lithium-Ion Batteries Via the Secondary Ion Mass Spectrometry

To develop lithium-ion batteries with a high rate-capability and low cost, the prevention of capacity loss is one of major challenges, which needs to be tackled in the lithium-ion battery industry. During electrochemical processes, lithium ions diffuse from and insert into battery electrodes accompanied with the phase transformation, whereas ionic diffusivity and concentration are keys to the resultant battery capacity. In the current study, we compare voltage versus capacity of lithium-ion batteries at different current-rates (C-rates) discharging. Larger hysteresis and voltage fluctuations are observed in higher C-rate samples. We investigate origins of voltage fluctuations by quantifying lithium-ion intensity and distribution via a time-of-flight secondary ion mass spectrometry (ToF-SIMS). The result shows that for fully discharged samples, lithium-ion intensity and distribution are not C-rate dependent, suggesting different lithium-ion insertion mechanisms at a higher C-rate discharging might be solely responsible for the observed low frequency voltage fluctuation. [DOI: 10.1115/1.4028010]

Keywords: lithium-ion batteries, secondary ion mass spectrometry, lithium-ion intensity

1 Introduction

Lithium-ion batteries are critical to modern and emerging technologies ranging from high-power tools and wearable electronics to prosthetic limbs and exoskeletons for the physically disabled. In enabling advanced plug-in hybrid (PHEV) and pure electric vehicles (EV), it is critical in the context of global climate change to meet mandates to reduce U.S. greenhouse gas emissions: a 17% reduction below 2005 levels by 2020 and an 83% reduction by 2050 [1], and doubling U.S. fuel efficiency from 27.3 miles per gallon (MPG) in 2011 to 54.5 MPG by 2025 [2]. Advancing lithium-ion battery technology for PHEVs/EVs and human quality-of-life enhancing technologies such as mechanized prosthetic limbs will play a critical role in fulfilling these goals. Toward providing the high power and energy densities demanded by these new technologies, fast discharging C-rates are considered essential [3]. However, at high C-rates, the capacity of current lithium-ion batteries decreases with increased charge/discharge cycles (referred to as "rate-capacity fade") [4]. Thus, cycling, C-rate, and concentration of lithium govern the capacity of lithium-ion batteries.

Among several developed cathode materials, the olivine-based lithium iron phosphate (LiFePO$_4$) with an orthorhombic crystal structure provides excellent characteristics for the application on EVs/PHEVs, such as good thermal stability, abundant iron ore resource, low raw material cost, and high theoretical energy density (170 mA h/g) [5–7]. At room temperature, LiFePO$_4$ works as a two-phase system [8], a lithium-rich (LiFePO$_4$) and a lithium-poor (FePO$_4$) phases during charging and discharging. The phase transformation of LiFePO$_4$ follows the Gibbs phase rule whereas a single-phase region has the characteristic of varying potentials with different lithium-ion concentrations, and a two-phase region reveals a steady potential during charging/discharging [9–11]. However, this characteristic of the flat charging/discharging curve is C-rate dependent and fluctuations in the scale of millivolt between the two-phase region are observed, especially under a higher C-rates (dis)charging [9–11]. Therefore, there is a need to further exam the origins causing voltage fluctuations, such as

lithium-ion intensity and distribution inside materials due to different C-rates (dis)charging.

To better detect the lithium-ion intensity from the surface to bulk materials, a ToF-SIMS is used [12–18]. ToF-SIMS is a highly sensitive surface analytical technique that can be used to detect atoms and molecules even at low concentrations down to the ppm level [12,19]. In general, ToF-SIMS is not a quantitative analytical method because many factors such as the ionization probability and matrix effect are varied for different species and samples. ToF-SIMS is generally used to establish depth profiles of elemental intensity based on the transport of particles. For example, Fedorkova et al. [14,20] have utilized ToF-SIMS to investigate the effect of conductive polymer polypyrrole (PPy) on the LiFePO$_4$ capacity, and they utilized the observed intensity distribution of Fe$^+$ and PPy to conclude that PPy is uniformly coated on particles. Li et al. [16] had used ToF-SIMS to investigate the depth profiles of solid-electrolyte-interphase (SEI) layers in Sn-Co anode materials during (dis)charging. They utilized the sputtering time required for the ToF-SIMS to observe volume expansion and shrinkage caused by the lithiation/delithiation. Similar phenomena were later observed in the Si-Ni alloy anodes [17] and ultrathin (<30 nm) Cr$_2$O$_3$ film anodes [18] from the same group.

In the current study, we first compare C-rate dependent voltage versus capacity relations for commercialized LiFePO$_4$ batteries. We then utilize a ToF-SIMS technique to quantify lithium-ion intensity and distribution inside these samples. We use LiFePO$_4$ as a model cathode material as LiFePO$_4$ is particularly well suited for the ToF-SIMS technique since LiFePO$_4$ contains the stable isotope ^{6}Li$^+$ and a high ion yield amenable to mass spectrometry techniques. Therefore, the investigation of lithium-ion intensity and distribution via a ToF-SIMS technique could potentially provide insight into electrochemical factors under different C-rate discharging.

2 Materials and Method

2.1 Charging/Discharging Experiments. It has been reported that lithium diffusion mechanism and phase transformation path might be C-rate dependent [9,10,21,22]. To compare the lithium-ion intensities under different C-rates (dis)charging, we first conduct the charging/discharging experiment. Commercial 26650 cylindrical LiFePO$_4$ lithium-ion batteries with a capacity of 2.5 A h

are used in the study. Totally eight cells are prepared and fully discharged at 1 C, 2 C, 6 C, and 10 C (two cells for each C-rate and 1 C = 2.5 A) to 0 V from a fully charged state (3.6 V). The charging/discharging experiments are conducted using an Arbin BT2000 cycler (Arbin Instrument, College Station, TX) at North Carolina State University. By referring to the experimental protocol for batteries for automotive applications [23], the following steps are used to conduct the charging/discharging experiment:

(1) Galvanostatically charge to 3.6 V at constant current I = 2.5 A.
(2) Switch to potentiostatic charging at constant voltage V = 3.6 V until the current drops to C/20 (0.125 A). The purpose of this step is to ensure the battery is fully charged.
(3) Discharge the batteries at different C-rates until the voltage drops to the recommended lower bound of the working voltage (2 V).
(4) Galvanostatically charge the battery at different C-rates to 3.6 V.

Steps (1)–(4) are repeated three times to ensure reproducibility of the voltage–time curve.

2.2 ToF-SIMS. After the cells are fully discharged to 0 V, we then disassemble them in a MBRAUN MB20G glove box system (M. Braun Inertgas-Systeme GmbH, Stratham, Germany) in the Analytical Instrumentation Facility at North Carolina State University. The glove box system is filled with nitrogen atmosphere to avoid the effect of air exposure [24]. The oxygen level in the glove box is maintained down to 1 ppm. Specifically, samples are kept in a nitrogen environment in a glove box at all times after the electrochemical measurements. Exposure to ambient air will be limited to 15 min during transport from the lab to the spectrometer. Based on a previous study, no additional oxide is expected to form in this 15 min period; further, a few tenths of a nanometer of air-derived ^{16}O oxide covering ^{17}O oxide have been shown not to affect such studies [25].

For each fully discharged cell (1 C, 6 C, and 10 C samples), we choose two different locations of the LiFePO₄ stripe for the subsequent ToF-SIMS analysis. The first location is chosen 10 cm from the edge of the unrolled LiFePO₄ stripe to avoid the edge effect. The second location is selected within a distance of 10 cm from the first spot, i.e., 20 cm from the edge of the stipe. For each spot, a sample size of approximately 1 mm × 1 mm is removed from the unrolled stripe and mounted on the sample holder that is later installed in the chamber of ToF-SIMS.

ToF-SIMS analyses are conducted by using an ION TOF SIMS V instrument (ION TOF, Inc., Chestnut Ridge, NY) in the Analytical Instrumentation Facility at North Carolina State University. The instrument vacuum system consists of a load lock for rapid sample loading connected by a gate valve to the analysis chamber. The analysis chamber pressure is maintained at or below 5.0×10^{-9} mbar to avoid contamination of the surfaces to be analyzed. ToF-SIMS is equipped with a Bi_3^+ liquid metal ion gun and a Cs^+ sputtering ion gun. Both the Bi and Cs ion columns are oriented at 45 deg with respect to the sample surface normal (Fig. 1). The sample surface is bombarded by a high-energy (~25 keV) primary ion-beam (e.g., Bi_3^+, Cs^+). The emitted secondary ions from the sample are then analyzed by calculating the flight time required to travel from the surface to the detector (Fig. 1).

Depth profile acquisition using ToF-SIMS is destructive due to the removal of sample material during the analysis. For such acquisition, the Cs^+ sputtering ion beam is rastered over an $80 \times 80 \ \mu m^2$ area to ablate a crater, and a 25 keV Bi_3^+ analysis beam is used to analyze a $10 \times 10 \ \mu m^2$ area on the crater bottom (Fig. 2). Specifically, while the Cs^+ ion beam ablates the material to generate a crater, the Bi_3^+ ion beam progressively analyzes the crater bottom. The two ion beams alternate to reveal elemental intensity as a function of depth, where we anticipate several
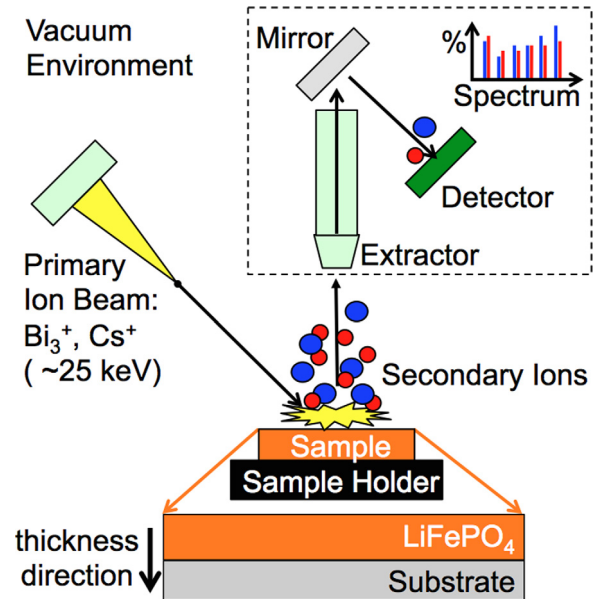
Fig. 1 Schematic of the ToF-SIMS technique for imaging lithium-ion intensity and distribution. The time required for atoms/molecules to hit the mass detector is calculated and the spectra of mass to charge ratio is obtained (inset).
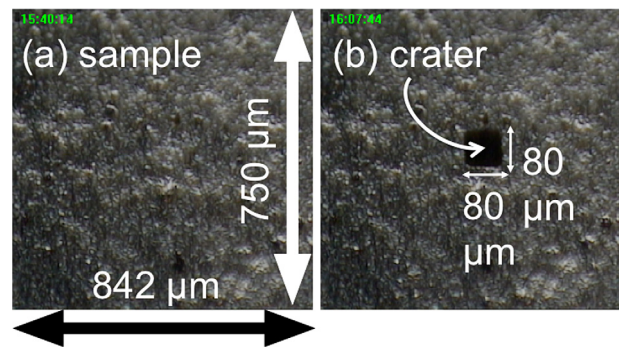

Fig. 2 Images of the sample surface (a) before and (b) after the sputtering process. The crater size is $80 \times 80 \ \mu m^2$, and the analysis area is $10 \times 10 \ \mu m^2$ in the middle of the sample to avoid the crater effects.

positive ion depth profiles are revealed. A higher intensity indicates a higher count of target ions that are detected by the detector during sputtering as shown in Fig. 1. An associated mass spectrum is also obtained and is used to compare the intensities of different atoms/molecules [12,19]. To quantify the lithium-ion intensity, ^6Li isotope (^6Li: ^7Li = 7.59%: 92.41% in nature) is used in the current study because the intensity of ^7Li exceeds the limit of the detector [26]. Of note, the depth-profiling mode of ToF-SIMS detects Fe^+ [27], rather than Fe^{2+} or Fe^{3+}. Crater depth is measured via a Tencor P-20 Stylus profilometer. The material removal rate of 4.4 nm/s during the ToF-SIMS process is then derived by using the crater depth (ca. 4500 nm) divided by the total sputtering time (1021 s).

3 Results and Discussion

3.1 Charging/Discharging Curves. Figure 3 depicts the voltage versus capacity curves we measured at different C-rates (1 C, 2 C, 6 C, and 10 C), where discharging curves are represented by solid lines and charging curves by dashed lines. The voltage gap (between charging and discharging) increases with increasing C-rate: for example, at a capacity = 0.015 (A h/g), the voltage
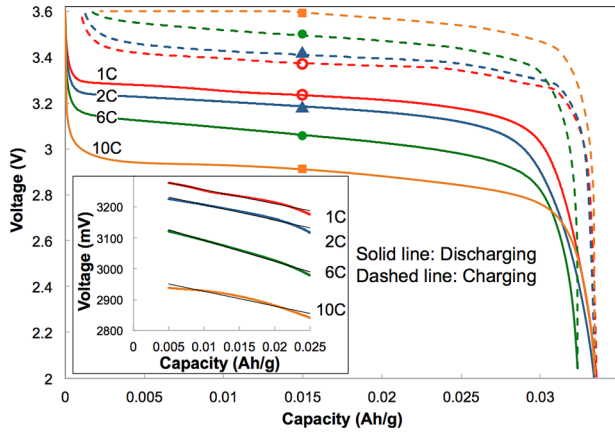
Fig. 3 Voltage versus capacity curves at different C-rates (1 C, 2 C, 6 C, and 10 C) for commercial 26650 cylindrical LiFePO₄ lithium-ion batteries. The voltage gap increases with increasing C-rate. Inset: linear trend lines between the capacities of 0.005 and 0.025 (A h/g). An increase in downward slope is observed from 1 C to 6 C. In addition, what appeared to be a low frequency (approx. 0.02 Hz) voltage fluctuation is observed in the 10 C sample. Note: The capacity is calculated based on the cell weight rather than pure electrode materials.

gaps are approximately 0.18 (V), 0.25 (V), 0.45 (V), and 0.68 (V) for 1 C, 2 C, 6 C, and 10 C, respectively (Fig. 3). The trend observed in these data is consistent with observations of Dreyer et al. [28]. Further, due to a characteristic of the two-phase system for LiFePO₄ materials, essentially flat voltage curves are observed for all C-rates. However, by comparing the discharging curves on a millivolt scale, we observe that the slopes of the voltage curves in this section are not identical, as shown in the inset of Fig. 3. An increasing downward slope of the curves is observed with higher C-rate, as well as what appears to be a subtle low frequency voltage fluctuation (approx. 0.02 Hz) for the 10 C sample, potentially offering additional evidence supporting previous observations that

an extra overpotential is required to overcome the energy barrier during the phase transformation of LiFePO₄ [28–30].

3.2 ToF-SIMS. The intensity of secondary elements is recorded through the sample thickness as the sputtering time progresses via ToF-SIMS. We report normalized intensity/counts depth profiles of two positive ions (i.e., Fe^+ and $^6Li^+$) at different C-rates, as shown in Fig. 4. Specifically, samples number 1 (#1) and number 2 (#2) are taken from the same cell while samples #3 and #4 are from the other cell. It is observed that most samples exists a peak profile around the depth = 0.4 μm and drops gradually. This peak is inferred to be the time required to reach the equilibrium during the sputtering process. As the cells are fully discharged before the ToF-SIMS analyses, most particles are already fully intercalated with lithium-ions. Therefore, $^6Li^+$ exhibits mostly constant depth-profile within the samples. It is also observed that the detected Fe^+ intensity/counts does not show a significant change through the thickness. It is due to the fact that Fe^+ remain in the crystalline during the (dis)charging process [31–33]. However, there are still some samples revealing fluctuations of the depth-profile in certain areas: 1 C sample #2 (between depth = 2 and 3 μm) and 6 C sample #4 (between depth = 3 and 4.5 μm). We speculate that the changes of the intensity/counts are due to the porosity inside the material. Any vacant area between two neighboring LiFePO₄ particles might cause a drop for both $^6Li^+$ and Fe^+ intensity/counts.

Figure 5 compares the ratio of $^6Li^+/Fe^+$ intensity at different C-rates by an interval of every 220 nm. It is observed that the depth-profile is not entirely C-rate dependent. It has revealed that 10 C samples have a higher ratio of $^6Li^+/Fe^+$ than that of 1 C and 6 C samples between depth = 3000 and 4500 nm, suggesting a higher intensity of $^6Li^+$ for the 10 C samples in this region. However, between the depth of 500 and 1000 nm, the ratio of $^6Li^+/Fe^+$ is less than one for most 1 C, 6 C, and 10 C samples, suggesting a $^6Li^+$ deficiency is observed on the material surface, rather than in the bulk material. The observed lithium deficiency near the sample surface is not C-rate dependent. For example, the ratio of $^6Li^+/Fe^+$ for 10 C at 880 nm is lower than that of 1 C and 6 C. However, the ratios of $^6Li^+/Fe^+$ for 10 C at 440 nm and 660 nm
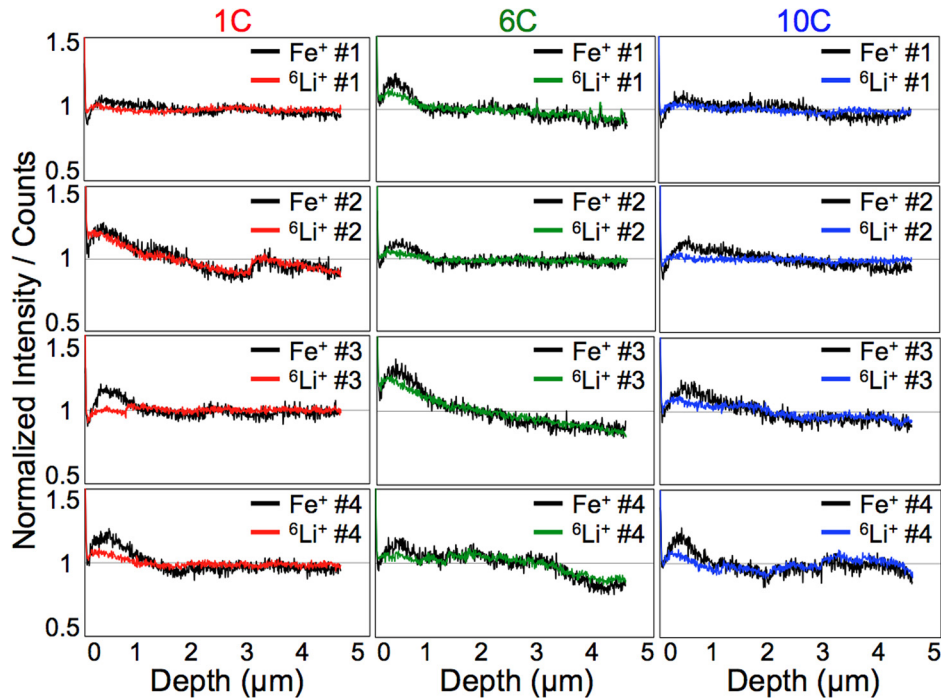
Fig. 4 Normalized intensity/counts depth-profiles of two positive ions (i.e., Fe^+ and $^6Li^+$) at different C-rates for each tested sample
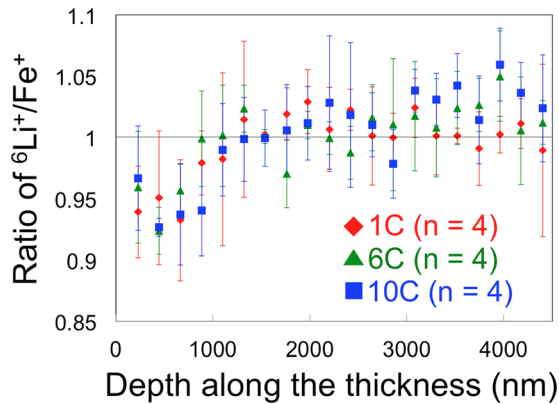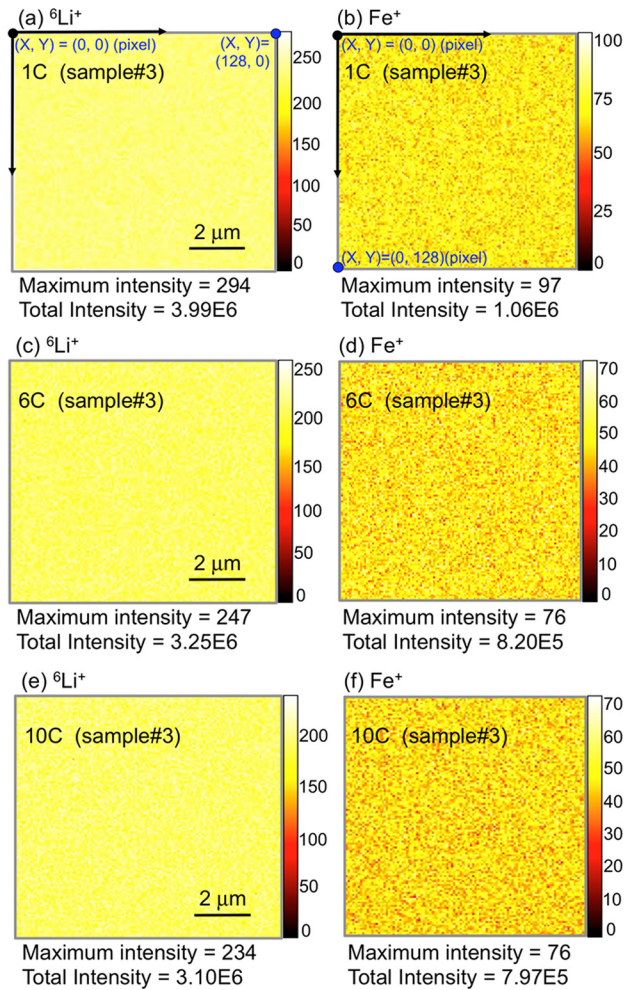
Fig. 5 Ratios of Li^+/Fe^+ measured at different C-rates and it is observed that the depth-profile is not entirely C-rate dependent. It is also observed that a $^6Li^+$ deficiency exists on the material surface (between the depth of 500 and 1000 nm), and it could be due to the removal of over-potential upon finishing discharging.

Fig. 6 ToF-SIMS images (128 μm × 128 μm) showing the intensity distribution of two positive ions (i.e., $^6Li^+$ and Fe^+) at different C-rates. (*a*) $^6Li^+$ and (*b*) Fe^+ intensity distributions of 1 C sample # 3. (*c*) $^6Li^+$ and (*d*) Fe^+ intensity distributions of 6 C sample # 3. (*e*) $^6Li^+$ and (*f*) Fe^+ intensity distributions of 10 C sample # 3. For different C-rate samples, similar maximum intensities of $^6Li^+$ (ca 250) and Fe^+ (ca 76) are observed, suggesting the intensity distribution is C-rate independent for fully discharged samples.

are in between 1 C and 6 C. An increased discharging C-rate does not cause an increased lithium deficiency near the electrode surface. Besides, the observed Li deficiency is not a constant since the ratio of $^6Li^+/Fe^+$ varies along the depth. One possible explanation for the observed lithium deficiency is proposed as follows: Lithium-ion in the host cathode material reaches the stoichiometry throughout the sample thickness when the cell is fully discharged. Once the overpotential is removed; however, a portion of lithium-ion diffuses back into the electrolyte. That is, the observed lithium-ion deficiency near the material surface (<1000 nm) is due to the removal of the over-potential upon finishing discharging, and it requires a higher driving force to further depleting of lithium-ions inside the bulk material. Another explanation for the observed lithium deficiency is possibly due to the formation of the SEI layer on the electrode surface. The formation of SEI layers on the cathode and anode surfaces has been observed for the $LiFePO_4$/Graphite batteries [34]. Zhong et al. have reported that the formation of the SEI layer will result in the depletion of lithium ions since Li_2CO_3 is one of the main compositions of SEI layers depositing on the cathode material. Thus, the observed the Li deficiency near the cathode surface might be due to the formation of SEI layers [34].

Song et al. [35] showed that the consumption of cycleable lithium ions is accompanied with the SEI layer formation, leading to a capacity loss after cycling for 18650-type $LiFePO_4$/Graphite cells. Their study shows that the capacity loss after cycling depends on the working temperature: The 5% and 30% capacity losses are observed after 600 cycling at 25 °C and 55 °C, respectively. A higher capacity loss is accompanied with a thicker SEI layer deposited on the graphite electrode. In contrast, the cells are disassembled after only three cycling in our study. Thus, the amount of lithium ion loss in the working electrode should be very small compared to the total cycleable lithium ions.

Representative ToF-SIMS images of the intensity distribution of two positive ions at different C-rates are shown in Fig. 6. Homogeneously distributed $^6Li^+$ and Fe^+ for three C-rate samples are observed, whereas there exist similar maximum intensities of $^6Li^+$ (ca 250) and Fe^+ (ca 76) in the samples. The total intensity sums over pixels where the cross section area 128 μm × 128 μm is considered. The concentration of $^6Li^+$ is estimated by using the intensity divided by the volume of the crater ($10 \times 10 \times 4.5 \, \mu m^3$). By using the data in Fig. 6, we could estimate lithium-ion concentration as follows: $C_{Li-1C} = 1.08 \times 10^{17}$, $C_{Li-6C} = 8.79 \times 10^{16}$, and $C_{Li-10C} = 8.38 \times 10^{16}$ (atoms/cm^3). These estimated concentrations from the current study are smaller than that reported in Nagpure et al., whereas a neutron depth profiling technique ($\sim 10^{20}$ atoms/cm^3) is adopted [26]. It is due to that ToF-SIMS is a

destructive analysis method thus the values are less than that derived from the neutron depth profiling technique.

From Figs. 3–6, it is noticed that the voltage fluctuation for the 10 C sample is more prominent comparing to other samples. It is suggested that for a multiparticle system, a factor such as lithium-ion insertion mechanisms might be related to the observed voltage fluctuation. Similar results were also concluded by Liu et al. [36]: have used high energy X-ray diffraction to measure the real-time structural changes during charging/discharging for commercial 18650 $LiFePO_4$ cells. The results show that the lithium intercalation mechanism is C-rate dependent and has been affected when the C-rate is increased from 0.1 C to 5 C. Based on their results, Liu et al. have also hypothesized that the lithium insertion mechanism and phase transformation pathway are C-rate dependent: the lithium insertion mechanism at higher C-rates becomes more a solid–solution pathway dominant.

4 Conclusion

In the present study, we first compare voltage versus capacity at different C-rates (1 C, 2 C, 6 C, 10 C) for $LiFePO_4$ materials. The voltage gap between charging and discharging increases while

increasing C-rate (dis)charging. The voltage fluctuation for the 10 C sample is more noticeable comparing to other samples. It is suggested that for a multiparticle system, additional factors such as lithium-ion insertion mechanisms, lithium-ion intensity, and distribution might be related to the observed voltage fluctuation.

Studies via a ToF-SIMS technique show that the $^6Li^+$ intensity depth profiles vary with the one of Fe^+, indicating that the intensity of Fe^+ could be used as an index for available $^6Li^+$ intercalation sites inside the material during discharging. Lithium-ion deficiency is observed in most samples near the sample surface (<1000 nm). It is possibly due to a portion of lithium-ion diffuse back into the electrolyte upon over-potential removal. The result from our current study also shows that for fully discharged samples, $^6Li^+$ intensity and distribution are not C-rate dependent. Thus different lithium-ion insertion mechanisms at a higher C-rate discharging might be solely responsible for the observed low frequency voltage fluctuation.

Acknowledgment

References

[1] Office of Atmospheric Programs, 2010, "Environmental Protection Agency Analysis of the American Power Act," U.S. Environmental Protection Agency, Washington, DC.

[2] Environmental Protection Agency and Department of Transportation, 2012, "2017–2025 Model Year Light-Duty Vehicle Greenhouse Gas Emissions and Corporate Average Fuel Economy Standards," Fed. Reg., 77(199), pp. 62627–62629.

[3] Chiang, Y., 2010, "Building a Better Battery," Science, 330(6010), pp. 1485–1486.

[4] Kang, B., and Ceder, G., 2009, "Battery Materials for Ultrafast Charging and Discharging," Nature, 458(7235), pp. 190–193.

[5] Yuan, L., Wang, Z., and Zhang, W., 2011, "Development and Challenges of LiFePO4 Cathode Material for Lithium-Ion Batteries," Energy Environ. Sci., 4(2), pp. 269–284.

[6] Park, M., Zhang, X., and Chung, M., 2010, "A Review of Conduction Phenomena in Li-Ion Batteries," J. Power Sources, 195(24), pp. 7904–7929.

[7] Zhang, W., 2011, "Structure and Performance of LiFePO4 Cathode Materials: A Review," J. Power Sources, 196(6), pp. 2962–2970.

[8] Yamada, A., Koizumi, H., and Nishimura, S., 2006, "Room-Temperature Miscibility Gap in LixFePO4," Nat. Mater., 5(5), pp. 357–360.

[9] Bai, P., Cogswell, D. A., and Bazant, M. Z., 2011, "Suppression of Phase Separation in LiFePO4 Nanoparticles During Battery Discharge," Nano Lett., 11(11), pp. 4890–4896.

[10] Cogswell, D. A., and Bazant, M. Z., 2012, "Coherency Strain and the Kinetics of Phase Separation in LiFePO4 Nanoparticles," ACS Nano, 6(3), pp. 2215–2225.

[11] Oyama, G., Yamada, Y., and Natsui, R., 2012, "Kinetics of Nucleation and Growth in Two-Phase Electrochemical Reaction of LixFePO4," J. Phys. Chem. C, 116(13), pp. 7306–7311.

[12] Belu, A., Graham, D., and Castner, D., 2003, "Time-of-Flight Secondary Ion Mass Spectrometry: Techniques and Applications for the Characterization of Biomaterial Surfaces," Biomaterials, 24(21), pp. 3635–3653.

[13] Castle, J. E., Decker, F., and Salvi, A. M., 2008, "XPS and TOF-SIMS Study of the Distribution of Li Ions in Thin Films of Vanadium Pentoxide After Electrochemical Intercalation," Surf. Interface Anal., 40(3–4), pp. 746–750.

[14] Fedorkova, A., Orinakova, R., and Orinak, A., 2011, "Electrochemical and TOF-SIMS Investigations of PPy/PEG-Modified LiFePO4 Composite Electrodes for Li-Ion Batteries," Solid State Sci., 13(5), pp. 824–830.

[15] Hong, T. E., Jeong, E. D., and Baek, S. R., 2012, "Nano SIMS Characterization of Boron- and Aluminum-Coated LiNi1/3Co1/3Mn1/3O2 Cathode Materials for Lithium Secondary Ion Batteries," J. Appl. Electrochem., 42(1), pp. 41–46.

[16] Li, J., Swiatowska, J., and Seyeux, A., 2010, "XPS and ToF-SIMS Study of Sn-Co Alloy Thin Films as Anode for Lithium Ion Battery," J. Power Sources, 195(24), pp. 8251–8257.

[17] Li, J., Swiatowska, J., and Maurice, V., 2011, "XPS and ToF-SIMS Study of Electrode Processes on Sn-Ni Alloy Anodes for Li-Ion Batteries," J. Phys. Chem. C, 115(14), pp. 7012–7018.

[18] Li, J., Maurice, V., and Swiatowska-Mrowiecka, J., 2009, "XPS, Time-of-Flight-SIMS and Polarization Modulation IRRAS Study of Cr2O3 Thin Film Materials as Anode for Lithium Ion Battery," Electrochim. Acta, 54(14), pp. 3700–3707.

[19] Swiatowska-Mrowiecka, J., Martin, F., and Maurice, V., 2008, "The Distribution of Lithium Intercalated in V2O5 Thin Films Studied by XPS and ToF-SIMS," Electrochim. Acta, 53(12), pp. 4257–4266.

[20] Fedorkova, A., Orinakova, R., and Orinak, A., 2010, "PPy Doped PEG Conducting Polymer Films Synthesized on LiFePO4 Particles," J. Power Sources, 195(12), pp. 3907–3912.

[21] Kao, Y., Tang, M., and Meethong, N., 2010, "Overpotential-Dependent Phase Transformation Pathways in Lithium Iron Phosphate Battery Electrodes," Chem. Mater., 22(21), pp. 5845–5855.

[22] Cogswell, D. A., and Bazant, M. Z., 2013, "Theory of Coherent Nucleation in Phase-Separating Nanoparticles," Nano Lett., 13(7), pp. 3036–3041.

[23] Zhang, Y., Wang, C., and Tang, X., 2011, "Cycling Degradation of an Automotive LiFePO4 Lithium-Ion Battery," J. Power Sources, 196(3), pp. 1513–1520.

[24] Martin, J. F., Yamada, A., and Kobayashi, G., 2008, "Air Exposure Effect on LiFePO4," Electrochem. Solid State Lett., 11(1) pp. A12–A16.

[25] Downing, R., Lamaze, G., and Langland, J., 1993, "Neutron Depth Profiling—Overview and Description of Nist Facilities," J. Res. Natl. Inst. Stand. Technol., 98(1), pp. 109–126.

[26] Nagpure, S. C., Downing, R. G., and Bhushan, B., 2011, "Neutron Depth Profiling Technique for Studying Aging in Li-Ion Batteries," Electrochim. Acta, 56(13), pp. 4735–4743.

[27] Williams, P., 1985, "Secondary Ion Mass-Spectrometry," Annu. Rev. Mater. Sci., 15, pp. 517–548.

[28] Dreyer, W., Jamnik, J., and Guhlke, C., 2010, "The Thermodynamic Origin of Hysteresis in Insertion Batteries," Nat. Mater., 9(5), pp. 448–453.

[29] Van der Ven, A., Garikipati, K., and Kim, S., 2009, "The Role of Coherency Strains on Phase Stability in LixFePO4: Needle Crystallites Minimize Coherency Strain and Overpotential," J. Electrochem. Soc., 156(11), pp. A949–A957.

[30] Malik, R., Zhou, F., and Ceder, G., 2011, "Kinetics of Non-Equilibrium Lithium Incorporation in LiFePO4," Nat. Mater., 10(8), pp. 587–590.

[31] Meethong, N., Kao, Y., and Tang, M., 2008, "Electrochemically Induced Phase Transformation in Nanoscale Olivines Li1-xMPO4 (M = Fe, Mn)," Chem. Mater., 20(19), pp. 6189–6198.

[32] Andersson, A., and Thomas, J., 2001, "The Source of First-Cycle Capacity Loss in LiFePO4," J. Power Sources, 97–98, pp. 498–502.

[33] Delmas, C., Maccario, M., and Croguennec, L., 2008, "Lithium Deintercalation in LiFePO4 Nanoparticles Via a Domino-Cascade Model RID G-6492-2011," Nat. Mater., 7(8), pp. 665–671.

[34] Zhong, K., Cui, Y., and Xia, X., 2014, "Study on the Stability of the LiFePO4 Li-Ion Battery Via an Electrochemical Method," J. Power Sources, 250, pp. 296–305.

[35] Song, H., Cao, Z., and Chen, X., 2013, "Capacity Fade of LiFePO4/Graphite Cell at Elevated Temperature," J. Solid State Electrochem., 17(3), pp. 599–605.

[36] Liu, Q., He, H., and Li, Z., 2014, "Rate-Dependent, Li-Ion Insertion/Deinsertion Behavior of LiFePO4 Cathodes in Commercial 18650 LiFePO4 Cells," ACS Appl. Mater. Interfaces, 6(5), pp. 3282–3289.